ChemPubSoc Europe

DOI: 10.1002/cbic.201402625

CHEMBIOCHEM Full Papers

Structure, Activity and Stereoselectivity of NADPH-Dependent Oxidoreductases Catalysing the *S*-Selective Reduction of the Imine Substrate 2-Methylpyrroline

Henry Man,[a] Elizabeth Wells,[a] Shahed Hussain,[b] Friedemann Leipold,[b] Sam Hart,[a] Johan P. Turkenburg,[a] Nicholas J. Turner,[b] and Gideon Grogan*[a]

Oxidoreductases from *Streptomyces* sp. GF3546 [3546-IRED], *Bacillus cereus* BAG3X2 (*Bc*IRED) and *Nocardiopsis halophila* (*Nh*IRED) each reduce prochiral 2-methylpyrroline (2MPN) to (*S*)-2-methylpyrrolidine with >95% *ee* and also a number of other imine substrates with good selectivity. Structures of *Bc*IRED and *Nh*IRED have helped to identify conserved active site residues within this subgroup of imine reductases that have *S* selectivity towards 2MPN, including a tyrosine residue that has a possible role in catalysis and superimposes with an aspartate in related enzymes that display *R* selectivity towards the same substrate. Mutation of this tyrosine residue—Tyr169—in 3546-IRED to Phe resulted in a mutant of negligible activity. The data together provide structural evidence for the location and significance of the Tyr residue in this group of imine reductases, and permit a comparison of the active sites of enzymes that reduce 2MPN with either *R* or *S* selectivity.

Introduction

Chiral amines are important entities in pharmaceutical chemistry, both as synthetic intermediates and as drug compounds themselves, and hence there has been a significant amount of research directed towards their asymmetric synthesis. Many of the approaches have used biocatalytic methods,[1] owing to the inherent asymmetric selectivity of enzymes, but also because of increasing pressure to adopt sustainable chemical technology in industrial pharmaceutical synthesis. Biocatalytic approaches to the asymmetric synthesis of amines have thus far included kinetic resolutions with hydrolases[2] and asymmetric transformations of a broad range of prochiral and racemic starting materials by use of a range of enzyme classes including transaminases,[3] amine oxidases[4] and amine dehydrogenases.[5]

A less well-explored route to asymmetric biocatalytic amine synthesis is through the reduction of prochiral imines, in a mode similar to that achieved for chiral alcohols through the reduction of prochiral ketones by ketoreductases (KREDs).[6] This would be a convenient synthetic route due to the use of prochiral imine substrates, which may be converted into the corresponding amines with a theoretical yield of 100% and with 100% *ee*. Some "imine reductase" (IRED) activities have been studied extensively in the past, if not for biocatalytic application; they include the enzymes dihydrofolate reductase (DHFR)[7,8] and pteridine reductase (PTR),[9,10] which reduces the C=N bond in pterin systems with the aid of NADPH as the hydride donor. More recently, a number of naturally occurring IREDs have also been applied in preparative biocatalytic synthesis.[11–19] The most interesting of these were identified by Mitsukura, Nagasawa and co-workers,[11–14] who screened a range of organisms for their ability to selectively reduce the commercially available cyclic imine 2-methylpyrroline (2MPN, **1**, Scheme 1).

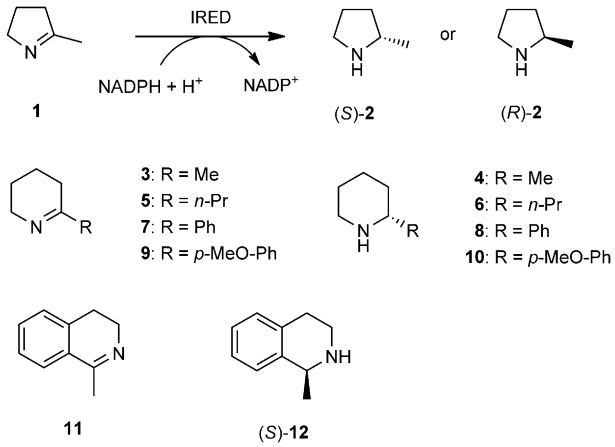

Scheme 1. Structures of substrates and products used in this study.

They discovered two strains, *Streptomyces* GF3587 and *Streptomyces* GF3546, which catalysed the reduction of **1** to the 2-methylpyrrolidine (amine) products (*R*)-**2** and (*S*)-**2**, respectively, with high enantiomeric excess. The Mitsukura group purified the enzymes responsible for these stereocomplementary reductions—"3587-IRED" (Uniprot code M4ZRJ3) and "3546-IRED"

[a] *H. Man, E. Wells, S. Hart, Dr. J. P. Turkenburg, Prof. Dr. G. Grogan*
Department of Chemistry, University of York
Heslington, York, YO10 5DD (UK)
E-mail: gideon.grogan@york.ac.uk

[b] *S. Hussain, Dr. F. Leipold, Prof. Dr. N. J. Turner*
Manchester Institute of Biotechnology, University of Manchester
131 Princess Street, Manchester, M1 7DN (UK)

Supporting information for this article is available on the WWW under http://dx.doi.org/10.1002/cbic.201402625.

(M4ZS15), respectively—and in subsequent papers also reported the cloning and heterologous expression in *Escherichia coli* of the genes that encode them.[12,14] These IREDs were shown to be dependent for activity exclusively on the nicotinamide cofactor NADPH, and to exist in solution as homodimers of monomers, each of approximately 30 kDa. Subsequently, Turner and co-workers have shown that cells of *E. coli* expressing 3546-IRED are able to catalyse the asymmetric reduction of a wide range of monocyclic and bicyclic imines, providing a biocatalyst with the potential for the preparation of chiral amine products.[15]

In previous work,[16] we determined the first X-ray crystal structure of an NADPH-dependent IRED demonstrated to have asymmetric imine reductase activity towards **1**. The structure of Q1EQE0 from *Streptomyces kanamyceticus*, which shares 50% sequence identity with 3587-IRED, was shown to be composed of an intimate dimer of monomers each displaying a two-domain structure: an N-terminal Rossman fold largely responsible for NADPH binding, and a C-terminal bundle. NADPH was observed bound at the interface between the N-terminal domain of the first subunit and the C-terminal domain of the second. The two domains were connected by a long interdomain helix, from which an aspartate residue—Asp187—projected into the active site towards the nicotinamide ring. Superposition of the Q1EQE0 structure with structurally related oxidoreductases of the hydroxyisobutyrate dehydrogenase family[20] suggested that Asp187 might be involved in the catalytic mechanism of imine reduction, and substitution of this residue for either an Asn or an Ala residue indeed removed the activity of Q1EQE0 towards **1** as measured by spectrophotometric assays of NADPH oxidation in the presence of **1**.

Now that the structure of an IRED that is *R*-selective for the reduction of 2MPN has been solved, it would be of interest to compare this to structures of homologues that are *S*-selective for reduction of this substrate. The structure of 3546-IRED has recently been reported,[17] but neither a detailed analysis of the active site, nor mutational studies on this enzyme as a representative member of enzymes with *S* selectivity towards 2MPN were presented. In this report we describe further studies on IREDs that catalyse the *S*-selective reduction of 2MPN, including the structures and activities of enzymes from *Bacillus cereus* BAG3X2-2 (*Bc*IRED) and *Nocardiopsis halophila* (*Nh*IRED). These data permit a comparison of IREDs that display stereocomplementary activity toward 2MPN. We also provide structural evidence for an active tyrosine residue, in place of an aspartate, as a possible residue involved in catalysis in this group of enzymes having *S* selectivity towards **1**, its location having previously only been suggested on the basis of modelling studies.[18]

Results and Discussion

Activity of homologues of 3546-IRED from *Streptomyces* sp. GF 3546

Three IREDs with *S* selectivity towards **1** were chosen for activity and structural studies: 3546-IRED from *Streptomyces* sp. GF 3546, *Bc*IRED from *B. cereus* BAG3X2-2 and *Nh*IRED from *N. halophila*. The genes encoding each IRED were synthesised with codon-optimisation for expression in *E. coli* and subcloned into the pETYSBLIC-3C vector.[21] The proteins, which were encoded with an N-terminal hexahistidine tag, were expressed in the soluble fraction of *E. coli* BL21(DE3) cells and purified by nickel affinity chromatography, followed by gel filtration.

The activity and stereoselectivity of 3546-IRED has been documented by Turner and co-workers,[15] and it has continued to serve as a model enzyme for mutational studies reported below. The first new enzyme was a putative IRED from *B. cereus* BAG3X2-2 (J7M26, *Bc*IRED). This enzyme shared 57% sequence identity with 3546-IRED and 78% similarity (Figure S1 in the Supporting Information). The purified enzyme (Figure S2) was challenged with six substrates in the presence of NADPH, and the results of the biotransformations are shown in Table 1.

Table 1. Results of biotransformations of imine substrates in Scheme 1 with IRED enzymes. Each reaction mixture (12 mL) contained 0.25 mg mL^{-1} of pure IRED and 5 mM substrate from a 0.25 M stock solution in DMF, with NADPH and cofactor recycling as detailed in the Experimental Section. Chiral chromatography traces for product analysis can be found in Figures S3–S8.

	Absolute configuration, conversion [%], enantiomeric excess [%]					
Enzyme	**1**	**3**	**5**	**7**	**9**	**11**
3546-IRED[a]	*S*, 57, 95	*S*, >98, 98	n.d.	n.d.	n.d.	*S*, 98, 98
BcIRED	*S*, 98, >99	*S*, 90, >99	*S*, 57, 35	*R*, 76, 63	*S*, 8, 18	*S*, 94, 81
*Nh*IRED	*S*, 80, >99	*S*, 86, >99	*R*, 90, 82	*S*, 100, 85	*S*, 53, 98	*S*, 97, 68

[a] Data taken from ref. [15], in which reactions were performed with whole cells of *E. coli*, expressing 3546-IRED. n.d. = not determined.

BcIRED catalysed the reduction of 1 to give the *S*-amine **2** as predicted, and also reduced 2-methylpiperidine (**3**) to amine (*S*)-**4**, each with >99% *ee*. Imines **5**, **7** and **9**, with increasingly larger groups in the 2-position, were reduced with lower levels of conversion and stereoselectivity. Conversion was very poor for substrate **9**. In the case of **7**, the stereoselectivity was formally reversed as a result of a switch according to the Cahn–Ingold–Prelog priority rules, but the product was still the result of hydride attack at the equivalent face of the imine substrate as for **1**. 1-Methyl-3,4-dihydroisoquinoline (**11**) was reduced to the *S*-amine with 94% *ee*.

Purified *Nh*IRED (Figure S2), from *N. halophila*, which shared 45% sequence identity with 3546-IRED, and 65% similarity, was also shown to reduce the panel of imine substrates, again with predominantly *S* selectivity. In contrast with *Bc*IRED, however, the activity and stereoselectivity with the larger substrates **5**, **7** and **9** were inverted (Table 1), with products now resulting from hydride attack from the opposite face to that

seen for **1** and **3**. Although unexpected, this result has many precedents in the history of alcohol dehydrogenase (ADH) biotransformations, with the selectivity of ADHs such as those from *Thermoanaerobium*[22] and *Sporobolomyces*,[23] for example, inverted when challenged with larger ketone substrates.

A comparison of the selectivity and activity of *Bc*IRED and *Nh*IRED with those of 3546-IRED[15] illustrates that the last enzyme displays better conservation of stereoselectivity towards **1**, **3** and **11** (Table 1). *Bc*IRED and *Nh*IRED are, however, slightly more active than 3546-IRED towards **1**, as determined by comparison of k_{cat}/K_m values, by factors of 0.5 and 6.0, respectively (Table 2).

Table 2. Kinetic constants determined for IRED enzymes and substrate 2MPN (**1**).

Enzyme	k_{cat} [s^{-1}]	K_m [mM^{-1}]	k_{cat}/K_m [$s^{-1} mM^{-1} \times 10^{-3}$]
3546-IRED[a]	0.024	11.82	2
*Bc*IRED	0.032	8.32	3
*Nh*IRED	0.013	1.10	11

[a] Data taken from ref. [15].

Structures of IRED homologues from *Bacillus* and *Nocardiopsis*

The structures of each of the IRED homologues were then determined by X-ray crystallography. The selection of multiple alternative enzymes for structural studies proved fruitful in respect of the acquisition of structures of IREDs that were *S*-selective for the reduction of **1**. A structure of 3546-IRED to a resolution of 3 Å was obtained, but during the preparation of this manuscript a structure at a superior resolution of 1.9 Å was published by Müller and co-workers[17] (PDB ID: 4OQY), so our data are not included here. The structure of *Bc*IRED was determined in two forms: an apo form to a resolution of 1.74 Å and a complex with NADPH that was determined to a resolution of 1.81 Å. Each *Bc*IRED structure was determined from crystals belonging to the $P2_12_12_1$ space group and featuring one dimer in the asymmetric unit. Details of the model can be found in Figure S9.

The structure of the apo form of BcIRED, again a dimer displaying the domain-swapping structure with an interdomain helix, superimposed with Q1EQE0—which has *R* selectivity towards **1**— with an overall rmsd of 1.8 Å. The *Bc*IRED dimer also superimposed with 3546-IRED (4OQY) with an overall rmsd of 2.6 Å. Each of these values was illustrative of the structural similarity within the wider IRED family of enzymes. Indeed, there were very few differences observed in secondary elements or tertiary structure throughout. The superimposition of *Bc*IRED with the Q1EQE0–NADPH complex (PDB ID: 3ZHB) also revealed that in place of Asp187 in Q1EQE0, which had been suggested to have a catalytic role in IRED catalysis in that enzyme, there was a tyrosine residue—Tyr188—at the "ceiling" of the NADPH-binding cleft and projecting into the proximal section of the NADPH binding site as presented in Figure 1 (right). Superimposition of *Bc*IRED with 3546-IRED (4OQY) also reveals a tyrosine residue (Tyr169) in an equivalent position.

The structure of *Bc*IRED complexed with NADPH in one active site displayed an rmsd with the apo structure of 1.3 Å, reflective of a perturbation on NADPH binding leading to a relative closure of the active site between the domains. The distance between, for example, the Cα atoms of Val138 and Met192, which are on opposite faces of the NADPH binding cleft on either side of the plane of the side chain Tyr188, closes from 12.6 to 11.8 Å. Such a perturbation was also observed for (*S*)-IRED by Müller and co-workers[17] and explains in part the larger rmsd for 3546-IRED in relation to *Bc*IRED, against the value in relation to Q1EQE0, in which no such movement was observed. On binding of NADPH, the side chain of Ser113 disengages from H-bonding contact with the side chain of Gln189 and His262 and rotates 180° to form an H-bond with the O2D oxygen of the NADPH ribose (at a distance of 3.0 Å), and also a weak H-bond (3.7 Å) with the phenolic hydroxy group of Tyr188. The side chain phenolic hydroxy group of Tyr188 itself is 5.0 Å from the C-4 atom of the nicotinamide ring of NADPH that donates hydride in the reductive reaction, and this compares well with the 5.2 Å observed in NADPH-dependent PTR, which is thought to employ Tyr194 as a proton donor to the nascent amine in the relevant reaction.[10] Other interactions with the cofactor are summarised in Figure S10. A discussion of further structural differences between the IREDs follows a description of the structure of *Nh*IRED.

The structure of *Nh*IRED was determined and refined to a resolution of 2.39 Å. Details of the model can be found in the Supporting Information (Figure S11).The rmsds between the

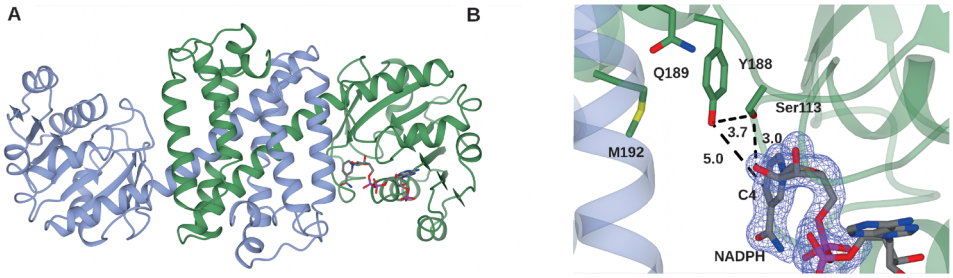

Figure 1. Structure of *Bc*IRED in complex with NADPH. Subunits **A** and **B** are shown in ribbon format in light blue and green, respectively. NADPH is shown in cylinder format with carbon atoms in grey at the dimer interface. Left: Structure of dimer. Right: Active site showing Tyr188 projecting towards the nicotinamide ring of NADPH. Residues are labelled with one-letter codes for clarity, and distances are given in Å. Electron density corresponds to the F_o-F_c (omit) map calculated in the absence of NADPH ligand and contoured at a level of 3 σ. NADPH atoms have been added for clarity.

dimer structure of this enzyme and those of *Bc*IRED, 3546-IRED and Q1EQE0 were 1.3, 2.3 and 1.9 Å, respectively. As in the cases of *Bc*IRED and 3546-IRED, a tyrosine residue—Tyr174—was observed to project into the putative NADPH binding cleft between domains. Although no complex of this *Nh*IRED with NADPH was forthcoming, the structure was determined in complex with the crystallisation detergent additive *n*-octyl β-D-glucoside (OBDG) within the active site (Figure 2, right). The detergent molecule participated in many active site interactions with residues including Tyr174, which was observed to form a H-bond at a distance of 2.7 Å from the 4-hydroxy group, whereas the 6-hydroxy group of the exocyclic hydroxymethyl system formed a H-bond of 3.1 Å in length with the side chain of Asn213. The *n*-octyl tail was bound in a hydrophobic region of the distal portion of the binding cleft, interacting with Phe181, Phe218, Trp182 and Phe282. These interactions are summarised in Figure S12. Despite the contact with Tyr174, it is unlikely that this represents a substrate-binding mode for this IRED, however, because the molecule is bound in the distal portion of the binding cleft as observed in Figure 2. In this location, the ligand projects away from the NADPH binding site, where the necessary interaction between the C-4 hydride of NADPH and the electrophilic carbon would take place. Indeed *Nh*IRED did not display any activity towards OBDG or its parent sugar (glucose) in spectrophotometric assays. The possibility that this complex is illustrative of a mode of entry for imine substrates cannot be excluded, however.

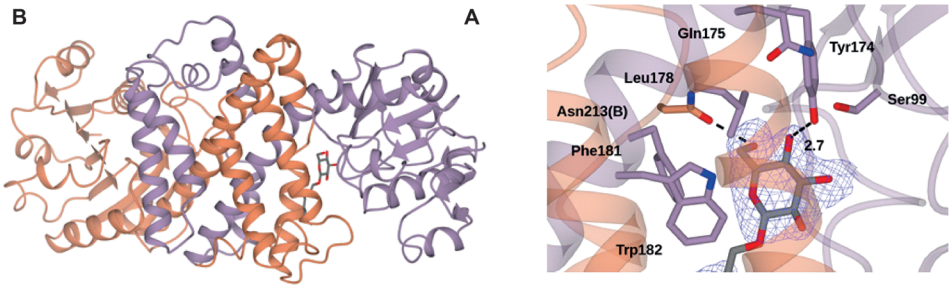

Figure 2. Structure of *Nh*IRED in complex with OBDG. Subunits **A** and **B** are shown in ribbon format in lilac and coral, respectively. OBDG is shown in cylinder format with carbon atoms in grey at the dimer interface. Left: Structure of dimer. Right: Active site showing Tyr174 projecting into the active site, together with H-bonding contacts of the ligand with residues at the active site. Residues are labelled with one-letter codes for clarity, and distances are given in Å. Electron density corresponds to the F_o-F_c (omit) map calculated in the absence of the OBDG ligand and contoured at a level of 3 σ. OBDG atoms have been added for clarity.

Conservation of active sites in structures of IREDs that are *S*-selective for the reduction of 2MPN

A sequence alignment of the IREDs discussed in this study, as well as of 3546-IRED and the enzymes Q1EQE0 and 3587-IRED, which are *R*-selective for 2MPN reduction, is given in the Supporting Information (Figure S1). Between *Bc*IRED, *Nh*IRED and 3546-IRED enzymes, an examination of the alignment and available structures confirmed that Tyr188 (*Bc*IRED), at the "ceiling" of the NADPH-binding cleft and projecting towards the nicotinamide ring of NADPH, is conserved in NhSIRED and 3546-IRED as Tyr174 and Tyr169, respectively, and also that it superimposed with Asp187 in Q1EQE0, Asp187 having been suggested to have a role in catalysis in that enzyme.[16] Further conserved residues adjacent to this Tyr, and within 6 Å of the side-chain phenol, include Gln189 (*Bc*IRED numbering), Ser113 as described previously, along with His262, with which it interacts in the apo form of *Bc*IRED, and Met192, which corresponds to Met173 in 3546-IRED, but to Leu178 in *Nh*IRED. Additionally, the phenolic hydroxy group of Tyr188 in *Bc*IRED is approximately 4.5 Å from the backbone carbonyl of a Val residue—Val138—conserved in both *Nh*IRED and 3546-IRED. The hydrophobic residues detailed as interacting with the tail of OBDG in *Nh*IRED are also conserved in both *Bc*IRED and 3546-IRED. In addition to Leu178, however, NhSIRED displays other differences from 3546-IRED and BcSIRED, such as Asp241, which corresponds to Gly in the other homologues. These substitutions might contribute to differences in selectivity observed between NhSIRED and the other enzymes for substrates with larger side chains.

Structural evidence for tyrosine as putative catalytic residue in IREDs that are *S*-selective for the reduction of 2MPN

Mutation of Asp187 to either Asn or Ala in Q1EQE0 resulted in mutants that displayed negligible activity towards **1** as determined by the standard UV assay of NADPH oxidation measured at 340 nm. The observed substitution of Asp for a Tyr residue in *Bc*IRED, *Nh*IRED and 3546-IRED prompted us to mutate the Tyr169 to Phe in 3546-IRED. This resulted in a mutant that also displayed negligible activity towards **1** in the standard UV assay. This is in agreement with a recent report by Hauer and co-workers, in which an equivalent Tyr residue in a homologue from *Paenibacillus elgii* was mutated to Ala to yield a largely inactive mutant.[18] These results suggest, by analogy with Q1EQE0, that this Tyr residue might have an active role in catalysis in 3546-IRED, *Bc*IRED and *Nh*IRED, perhaps as proton donor to the nascent amine in the reductive reaction. Certainly Tyr has been shown to fulfil a similar role in other imine reductases such as NADPH-dependent PTR[10] and also in sugar dehydrogenases such as xylose–xylitol reductase.[24,25] The side-chain phenolic hydroxy group of Tyr188 in *Bc*IRED itself is 5.0 Å from the C-4 atom of the nicotinamide ring of NADPH that donates hydride in the reductive reaction, and this compares well with the distances of 5.2 and 4.6 Å observed for relevant interactions in PTR and xylose–xylitol reductase, respectively. In PTR, however, the active site environment is somewhat different, because the Tyr side chain is part of a triad in which it interacts with a lysine residue that might have a role in lowering

the pK_a of the Tyr and stabilising the transition state of the reaction, as well as an aspartate residue that might be a proton donor to Tyr.[10] In fact, PTR exhibits a pH optimum for activity of 4.7–6.0 depending on the substrate,[9] whereas the pH optimum for 3546-IRED activity with **1**, for example, was determined to be approximately 7.5 (Figure 3), with the midpoint of the declining alkaline slope at approximately 8.0, indicative of a higher pK_a for the Tyr in IRED catalysis by that enzyme.

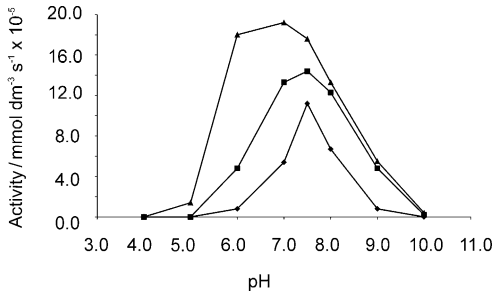

Figure 3. pH optima of IREDs illustrated by the activity of "tyrosine" IRED 3546-IRED (◆) and "aspartate" IREDs Q1EQE0 (■) and 3587-IRED (▲), assayed against 2MPN (**1**).

Interestingly, the pH activity profile of the tyrosine-containing 3546-IRED is different from those of the aspartate-containing IREDs (Figure 3), which exhibit a broader range of activity overall, together with pK_a values suggested by the midpoint of the declining alkaline slope of 8.5 (Figure 3), high for an aspartate, but similar to that reported for the aspartate-dependent IRED *E. coli* dihydrofolate reductase.[26]

The high pK_a values for the aspartate residues in Q1EQE0 and 3587-IRED are not unexpected because the aspartate is in each case held within a hydrophobic pocket formed by Ala135, Leu137 and Leu191 (Q1EQE0 numbering), the first two of which are not conserved as hydrophobic residues in 3546-IRED and homologues. Also, in Q1EQE0 the aspartate is 7.9 Å from the NADPH C4 atom, similar to the equivalent distance in DHFR, in which a network of hydrogen bonds through the substrate, rather than direct proton transfer, is implicated in the protonation of the nascent amine in the reductive reaction. Overall, an interesting analogy can therefore be made between the tyrosine-containing IREDs and the aspartate-containing IREDs, in which the distance between the putative "proton donor" and the NADPH C4 atom might provide clues to possible contributions to mechanism; in the former case there is crystallographic evidence from PTR to suggest that proton donation is directly from the side chain, whereas in the latter case the consensus on DHFR now appears to be that although the aspartate residue indeed assists in catalysis (and is buried in a hydrophobic hole as in Q1EQE0), its role is as part of an H-bonding network that assists the role of a water molecule in donation of the proton to the nitrogen atom. The clarification of these mechanistic aspects awaits the structures of both classes of IRED in complex with imine substrates.

Comparison of active sites of IREDs that are stereocomplementary for the reduction of 2MPN

A superimposition of the active sites of *Bc*IRED and Q1EQE0, which are specific for the *S*- and *R*-selective reductions of 2MPN, respectively, is shown in Figure 4. Truncated forms of

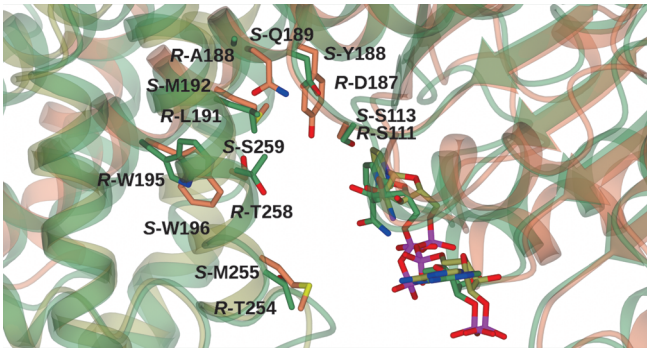

Figure 4. Superimposition of Q1EQE0 (green ribbons) with *Bc*IRED (coral). Carbon atoms of side chains and of NADPH are shown in green and coral, respectively. Residues are labelled with one-letter codes for clarity and with the prefix designations "*R*" (e.g., *R*-D187) for Q1EQE0 and "*S*" (e.g., *S*-Y188) for *Bc*IRED indicative of their selectivity for 2MPN.

the structures that featured only 85 residues of the secondary elements completing the active site cleft superimposed with an rmsd of 1.3 Å, lower than that for whole dimer. Coupled with the sequence alignment, a comparison of the *Bc*IRED structure with that of Q1EQE0 shows that, apart from the replacement of Tyr188 with Asp187, Met255 (*Bc*IRED) is replaced by Thr254 (Q1EQE0), Trp196 is conserved as Trp195, and Ser259 is replaced by Thr258 (Figure 4).

Gly256 in BcSIRED (not shown) is a His residue both in Q1EQE0 and also in 3587-IRED. From the sequences and structures, all of the determinants of NADPH binding in *Bc*IRED, *Nh*IRED, 3546-IRED and Q1EQE0 appear to be conserved, and the cofactor-binding loops are very similar, with the *re*-face of the nicotinamide ring stacking against a Met residue (Met33 in *Bc*IRED) in all cases, the O2 atom of ribose bound by Ser113, and the 2′-ribose hydroxy phosphate on NADPH secured by a phosphate-binding loop with interactions to Arg53, Thr54 and Lys57 as part of a conserved R53TXXK motif in all enzyme structures.

The comparison detailed above shows that there is remarkably little difference within the active sites of IREDs that display stereocomplementary behaviour towards the model substrate 2MPN, even within the region at or near the site between C4 of the nicotinamide cofactor and the putative "catalytic" active site residue, either Asp or Tyr in each case. One way in which to examine the structural basis for stereocomplementary behaviour would be to compare the sequences of enzymes of *S* and *R* selectivity towards 2-MPN, to perform reciprocal mutations at sites in the NADPH binding cleft, and to assess their altered stereoselective behaviour. However in the case of IREDs, simple reciprocal mutation of residues might be uninformative, owing to probable contributions to catalysis from neighbour-

ing residues. Such reciprocal mutations on enzymes 3587-IRED and 3546-IRED have met with limited success: mutation of Asp172 (Asp187 in Q1EQE0) to Tyr in 3587-IRED and of Tyr169 to Asp in 3546-IRED have led to poor expression and/or insoluble expression of the mutants (data not shown). Among other residues, the mutation of Met236 in 3546-IRED (conserved as Met255 in *Bc*IRED and shown at the opening of the active site in Figure 4) to the Thr residue found in 3587-IRED also resulted in insoluble protein. Conversely, mutation of Thr241 (Thr254 in Q1EQE0) in 3587-IRED to a Met residue gave mutant Thr241Met, which converted the substrate 2MPN to the *R* product **2** with 95% *ee*, much as was observed for the wild type. The currently available structures of IREDs suggest that it is probable that IRED stereoselectivity is governed by complex interactions that might include not only the environment created by the amino acid side chains in the active site, but also domain motions that are hinted at in the relative movements between domains observed in *Bc*IRED on NADPH binding. It is also the case that the known structures of IREDs represent only a small fraction of IRED sequences now available, and that the phenomena observed for known enzymes might not be generally observed throughout the IRED family.

Conclusions

Imine reductases (IREDs) provide promising new biocatalysts for the asymmetric production of chiral amines. The future exploitation of these enzymes should benefit greatly from structural investigations that help to reveal the molecular bases of mechanism and selectivity. They should also provide a rational basis for the engineering of IREDs for altered or improved activities in the future.

Experimental Section

Chemicals: Chemicals, including commercially available substrates, cofactors and buffer and media components, were purchased in general from Sigma–Aldrich. Imine substrates and products were synthesised as described in ref. [15]. Substrates **3**, **5**, **7**, **9** and **11** and amine products **2**, **4**, **6**, **8**, **10** and **12** were also synthesised as reported in ref. [15].

Gene synthesis, cloning, expression and protein purification: The genes encoding 3546-IRED, 3587-IRED, *Bc*IRED and *Nh*IRED were synthesised by GeneArt (Invitrogen), with the sequence optimized by use of the GeneArt server programme for expression in *E. coli*. For subcloning, the genes were amplified by PCR from the received plasmids containing the synthetic genes with use of the primers detailed in Table S1. After analysis of the PCR on agarose gels, bands of the appropriate size were isolated from the gel with the aid of a PCR Cleanup kit (Qiagen). Genes were then sub-cloned into the pET-YSBL-LIC-3C vector by a previously published procedure.[21] The resultant recombinant vectors were used to transform *E. coli* XL1-Blue cells (Novagen), yielding colonies that in turn gave plasmids through the use of standard miniprep procedures that were sequenced to confirm the identities and sequences of the genes. Mutant genes 3546-IRED Tyr169Phe, 3546-IRED Met236Thr and 3587-IRED Thr241Met were generated by use of a Quikchange kit from Agilent according to the manufacturer's instructions. The incorporation of mutations was then verified by DNA sequencing.

For gene expression, recombinant vector(s) containing IRED genes and mutants were used to transform *E. coli* BL21(DE3), and resultant colonies were grown overnight on lysogeny broth (LB) agar with kanamycin (30 $\mu g\,mL^{-1}$) as antibiotic marker. One colony of the relevant recombinant strain was used to inoculate a starter culture of LB medium (5 mL) containing kanamycin (30 $\mu g\,mL^{-1}$). This was then grown for 18 h with shaking at 180 rpm at 37 °C. The turbid starter culture was used to inoculate larger volumes of LB broth (500 mL) containing kanamycin (30 $\mu g\,mL^{-1}$) in a 2 L Erlenmeyer flask, in which cells were grown until the OD_{600} had reached a value of 0.6. The expression of IRED genes and mutants was induced at this point by the addition of isopropyl β-D-1-thiogalactopyranoside (IPTG, to a final concentration of 1 mM). Cultures were then grown in an orbital shaker at 180 rpm at 18 °C for 18 h. After this time, cell cultures were centrifuged at 4225 *g* for 15 min in a Sorvall GS3 rotor in a Sorvall RC5B Plus centrifuge. Cell pellets were resuspended in Tris·HCl buffer ("buffer", 50 mM, pH 7.5, 25 mL per L of cell growth) that also contained sodium chloride (300 mM). The cell suspensions were sonicated for 3×30 s bursts at 4 °C with 1 min intervals.

The insoluble and soluble fractions were separated by centrifugation at 26892 *g* in a Sorvall SS34 rotor for 30 min. The supernatants were filtered through a 2 μm Amicon filter and were then loaded onto a 5 mL His-Trap Chelating HP column. The columns were washed with five column volumes of buffer containing imidazole (30 mM), and IRED proteins and mutants were eluted with an imidazole gradient (30–500 mM) over twenty further column volumes. Fractions containing IREDs were identified by analysis by SDS-PAGE and pooled. These were then concentrated by use of a 10 kDa cut-off Centricon filter membrane. Concentrated IREDs were then loaded onto an S75 Superdex 16/60 gel filtration column that had been pre-equilibrated with buffer. The columns were then eluted with buffer at a flow rate of 1 $mL\,min^{-1}$. Fractions containing pure IREDs or mutants as determined by SDS-PAGE analysis were pooled and stored at 4 °C.

Protein crystallisation: Pure *Bc*IRED and *Nh*IRED were subjected to crystallisation trials with use of a range of commercially available screens in 96-well sitting-drop format in which each drop consisted of protein (150 nL) and precipitant reservoir solution (150 nL). For *Bc*IRED, initial crystals were obtained in PEG 3350 (25%, *w*/*v*), $MgCl_2$ (0.2 M), and HEPES (0.1 M) at pH 7.5, with protein at a concentration of 50 $mg\,mL^{-1}$. For *Nh*IRED, initial crystals were obtained in PEG 3350 (18%, *w*/*v*), $MgCl_2$ (0.25 M) and Bis–Tris (0.1 M) at pH 5.5, with protein at a concentration of 60 $mg\,mL^{-1}$. Larger crystals for diffraction analysis under optimised conditions were prepared by the hanging-drop method in 24-well plate Linbro dishes with 2 mL drops consisting of a 1:1 ratio of mother liquor to protein. For *Bc*IRED the best crystals were obtained in PEG 3350 (30%, *w*/*v*), $MgCl_2$ (0.2 M) and HEPES (0.1 M) at pH 7.5 after 3 months at 18 °C. For *Nh*IRED, the best crystals were obtained in OBDG (1%, *w*/*v*), PEG 3350 (18%, *w*/*v*), $MgCl_2$ (0.25 M) and Bis–Tris (0.1 M) at pH 5.5 after 2 months at 18 °C.

For both enzymes, co-crystallisation with NADPH (10 mM) did not yield crystals under the same buffer conditions. In order to obtain the NADP(H) complex of *Bc*IRED, native crystals were transferred from the growth drop into a cryogenic solution consisting of the mother liquor containing ethylene glycol (20%, *v*/*v*) and NADPH (20 mM) and incubated for 1 h, after which they were immediately flash-cooled in liquid nitrogen. Native crystals of both *Bc*IRED and *Nh*IRED were flash-cooled in a cryogenic solution containing only the mother liquor and ethylene glycol (10%, *v*/*v*). All crystals were tested for diffraction in-house with a Rigaku Micromax-007HF in-

strument fitted with Osmic multilayer optics and a Marresearch MAR345 imaging plate detector. Those crystals that diffracted to a resolution of equal to, or better than, 3 Å resolution were retained for dataset collection at the Diamond synchrotron.

Data collection, structure solution, model building and refinement of BcIRED and *Nh*IRED: Complete datasets described in this report were collected at Diamond Light Source, Didcot, Oxfordshire, UK. The *apo-Bc*IRED and the *Nh*IRED complex with OBDG were collected on beamline I04-1, and the *Bc*IRED NADPH complex on beamline I04. Data were processed and integrated by use of XDS[27] and scaled by using SCALA[28] included in the Xia2 processing system.[29] Data collection statistics are given in Table S2.

In each case the crystals of *Bc*IRED were in space group $P2_12_12_1$. The structure of *Bc*IRED was solved with MOLREP,[30] by use of a monomer model of the IRED Q1EQE0, PDB ID: 3ZGY. The solution(s) each contained two molecules in the asymmetric unit, representing one dimer. The solvent content in each case was 60%. The structures were built and refined by use of iterative cycles with Coot[31] and REFMAC,[32] the latter employing local NCS restraints. For the NADPH complex of *Bc*IRED, after building and refinement of the protein and water molecules, clear residual density was observed in the omit maps at one of the subunit dimer interfaces. This was modelled and refined as NADPH. The final structures exhibited R_{cryst} and R_{free} values of 17.6 and 21.7 (apo) and 23.2 and 30.0% (NADPH complex), respectively. For *Nh*IRED, the crystals were in space group $P2_12_12$, and had eight molecules in the asymmetric unit, representing four dimers. The solvent content in this case was 50%. The structure was again solved with MOLREP by use of a monomer of Q1EQE0 as a search model, and was built and refined as for *Bc*IRED. Four dimers featured in the asymmetric unit. After building and refinement, clear omit map density was again observed at the NADPH-biding site at the dimer interface, but was clearly not NADPH. It was successfully modelled as the crystallisation additive OBDG (*n*-octyl β-D-glucoside). The final structure exhibited R_{cryst} and R_{free} values of 23.0 and 26.6. All structures were finally validated with PROCHECK.[33] Refinement statistics for all structures are presented in Table S2. The Ramachandran plot for the apo-*Bc*IRED showed 97.5% of residues to be situated in the most favoured regions, 1.8% in additional allowed and 0.7% residues in outlier regions. For the NADPH complex, the corresponding values were 97.5, 2.1 and 0.4% respectively. For *Nh*IRED the values were 96.3, 2.6 and 1.1%. The coordinates and structure factors for the *Bc*IRED, the *Bc*IRED NADPH complex and *Nh*IRED have been deposited in the Protein Data Bank with the accession codes 4D3D, 4D3F and 4D3S, respectively.

Enzyme assays: The NADPH-dependent imine reductase activity of recombinant IREDs and mutants in this study was assessed as previously for Q1EQE0 by means of UV spectrophotometry.[16] Activity was determined with a Spectramax M2 spectrophotometer/plate reader (Molecular Devices) by monitoring the decrease in NADPH at 340 nm ($\varepsilon = 6.22\ mM^{-1}cm^{-1}$) for substrate 2MPN (**1**). Activity was determined with microtest plates (Sterilin, Newport, UK). Reaction mixtures (0.2 mL) contained pure enzyme (0.3 mg), NADPH (750 μM) and the appropriate amount of substrate (2 μL) from a 100-fold concentrated stock in DMSO. The reaction was started by adding the enzyme to the mixture. One unit of imine reductase is defined as the amount of protein that oxidized 1 μmol NADPH per minute. Kinetic parameters were determined with purified enzyme and analysed by nonlinear regression analysis based on Michaelis–Menten kinetics with use of the program QtiPlot.

Biotransformations: Biotransformations of substrates **1**, **3**, **5**, **7**, **9** and **11** were performed with the purified enzyme(s) or mutants and NADPH recycling by the method described previously.[16] Reactions were each performed in a 12 mL total reaction volume containing pure IRED (0.25 mg mL^{-1}) and substrate (5 mM) from a stock solution in DMF (0.25 M). The final concentration of dimethylformamide in the reaction was 2% (*v*/*v*). For cofactor recycling, NADPH (5 mg, 0.006 mmol), glucose-6-phosphate (3.5 mg, 0.013 mmol) and a glucose-6-phosphate dehydrogenase suspension (G8404 from Sigma–Aldrich, 12 μL per mL of total reaction volume) were added. After the overnight reaction at 30 °C, 500 μL of the mixture was removed, quenched with sodium hydroxide (10 M, 30 μL) and extracted with dichloromethane (2×500 μL). Samples (100 μL) of biotransformations of **1**, **3**, **5** and **7** were derivatised by *N*-acetylation with acetic anhydride and triethylamine and analysed by GC as described in the Supporting Information. Samples of biotransformations of **9** and **11** were analysed directly by HPLC as detailed in ref. [15]. Chiral analysis of products was performed as detailed in Figures S3–S8, which contain illustrative chromatograms for the separation of enantiomers of products **2**, **4**, **6**, **8**, **10** and **12**.

Acknowledgements

We thank the industrial affiliates of the Centre of Excellence for Biocatalysis, Biotransformations and Biomanufacture (CoEBio3) for awarding studentships to H.M. and E.W. S.H. was supported by a CASE studentship with AstraZeneca. F.L. received funding from the European Union's Seventh Framework Programme FP7/2007–2013 under grant agreement n° 266025 (BIONEXGEN).

Keywords: amines · asymmetric catalysis · imines · IREDs · NADPH · oxidoreductases

[1] M. Höhne, U. T. Bornscheuer, *ChemCatChem* **2009**, *1*, 42–51.
[2] S. Buchholz, H. Gröger, *Biocatalysis in the Pharmaceutical and Biotechnology Industries* (Ed.: R. N. Patel), CRC, London, **2006**, pp. 829–847.
[3] S. Mathew, H. Yun, *ACS Catal.* **2012**, *2*, 993–1001.
[4] D. Ghislieri, A. P. Green, M. Pontini, S. C. Willies, I. Rowles, A. Frank, G. Grogan, N. J. Turner, *J. Am. Chem. Soc.* **2013**, *135*, 10863–10869.
[5] M. J. Abrahamson, E. Vázquez-Figueroa, N. B. Woodall, J. C. Moore, A. S. Bommarius, *Angew. Chem. Int. Ed.* **2012**, *51*, 3969–3972; *Angew. Chem.* **2012**, *124*, 4036–4040.
[6] M. M. Musa, R. S. Phillips, *Catal. Sci. Technol.* **2011**, *1*, 1311–1323.
[7] D. R. Smith, J. M. Calvo, *Nucleic Acids Res.* **1980**, *8*, 2255–2274.
[8] M. R. Sawaya, J. Kraut, *Biochemistry* **1997**, *36*, 586–603.
[9] B. Nare, L. W. Hardy, S. M. Beverley, *J. Biol. Chem.* **1997**, *272*, 13883–13891.
[10] D. G. Gourley, A. W. Schuttelkopf, G. A. Leonard, J. Luba, L. W. Hardy, S. M. Beverley, W. N. Hunter, *Nat. Struct. Mol. Biol.* **2001**, *8*, 521–525.
[11] K. Mitsukura, M. Suzuki, K. Tada, T. Yoshida, T. Nagasawa, *Org. Biomol. Chem.* **2010**, *8*, 4533–4535.
[12] K. Mitsukura, M. Suzuki, S. Shinoda, T. Kuramoto, T. Yoshida, T. Nagasawa, *Biosci. Biotechnol. Biochem.* **2011**, *75*, 1778–1782.
[13] T. Nagasawa, T. Yoshida, H. Yamamoto, N. Kimoto (Daicel Chemical Industries, Ltd.), US Patent Application 20110287494, **2009**.
[14] K. Mitsukura, T. Kuramoto, T. Yoshida, N. Kimoto, H. Yamamoto, T. Nagasawa, *Appl. Microbiol. Biotechnol.* **2013**, *97*, 8079–8086.
[15] F. Leipold, S. Hussain, D. Ghislieri, N. J. Turner, *ChemCatChem* **2013**, *5*, 3505–3508.
[16] M. Rodríguez-Mata, A. Frank, E. Wells, F. Leipold, N. J. Turner, S. Hart, J. P. Turkenburg, G. Grogan, *ChemBioChem* **2013**, *14*, 1372–1379.
[17] T. Huber, L. Schneider, A. Präg, S. Gerhardt, O. Einsle, M. Müller, *ChemCatChem* **2014**, *6*, 2248–2252.

[18] P. N. Scheller, S. Fademrecht, S. Hofelzer, J. Pleiss, F. Leipold, N. J. Turner, B. M. Nestl, B. Hauer, *ChemBioChem* **2014**, *15*, 2201 – 2204.
[19] M. Gand, H. Müller, R. Wardenga, M. Höhne, *J. Mol. Catal. B* **2014**, *110*, 126 – 132.
[20] N. K. Lokanath, N. Ohshima, K. Takio, I. Shiromizu, C. Kuroishi, N. Okazaki, S. Kuramitsu, S. Yokoyama, M. Miyano, N. Kunishima, *J. Mol. Biol.* **2005**, *352*, 905 – 917.
[21] K. E. Atkin, R. Reiss, N. J. Turner, A. M. Brzozowski, G. Grogan, *Acta Crystallogr. Sect. F Struct. Biol. Cryst. Commun.* **2008**, *64*, 182 – 185.
[22] E. Keinan, E. K. Hafeli, K. K. Seth, R. Lamed, *J. Am. Chem. Soc.* **1986**, *108*, 162 – 169.
[23] D. Zhu, L. Hua, *J. Org. Chem.* **2006**, *71*, 9484 – 9486.
[24] B. Petschacher, S. Leitgeb, K. L. Kavanagh, D. K. Wilson, B. Nidetzky, *Biochem. J.* **2005**, *385*, 75 – 83.
[25] A. H. Ehrensberger, R. A. Elling, D. K. Wilson, *Structure* **2006**, *14*, 567 – 575.
[26] E. Ohmae, Y. Miyashita, S.-I. Tate, K. Gekko, S. Kitazawa, R. Kitahara, K. Kuwajima, *Biochim. Biophys. Acta Proteins Proteomics* **2013**, *1834*, 2782 – 2794.
[27] W. Kabsch, *Acta Crystallogr. Sect. D Biol. Crystallogr.* **2010**, *66*, 125 – 132.
[28] P. Evans, *Acta Crystallogr. Sect. D Biol. Crystallogr.* **2006**, *62*, 72 – 82.
[29] G. Winter, *J. Appl. Crystallogr.* **2010**, *43*, 186 – 190.
[30] A. Vagin, A. Teplyakov, *J. Appl. Crystallogr.* **1997**, *30*, 1022 – 1025.
[31] P. Emsley, K. Cowtan, *Acta Crystallogr. Sect D Biol. Crystallogr.* **2004**, *60*, 2126 – 2132.
[32] G. N. Murshudov, A. A. Vagin, E. J. Dodson, *Acta Crystallogr. Sect. D Biol. Crystallogr.* **1997**, *53*, 240 – 255.
[33] R. A. Laskowski, M. W. Macarthur, D. S. Moss, J. M. Thornton, *J. Appl. Crystallogr.* **1993**, *26*, 283 – 291.

Received: October 27, 2014
Published online on March 24, 2015